

1996 IEEE INTERNATIONAL FREQUENCY CONTROL SYMPOSIUM
REDUCING THE NORMAL ACCELERATION SENSITIVITY OF SURFACE TRANSVERSE WAVE
RESONATORS USING MICROMACHINED ISOLATION SYSTEMS

J. Robert Reid and Victor M. Bright
Department of Electrical and Computer Engineering
Air Force Institute of Technology
Wright-Patterson AFB, OH 45433-7765

Jim T. Stewart and John A. Kosinski
U.S. Army Research Laboratory
Physical Sciences Directorate
AMSRL-PS-ED
Fort Monmouth, NJ 07703

Abstract Micromachined silicon platforms provide two methods for reducing the acceleration sensitivity of surface transverse wave resonators. First, micromachining allows precise control over the structure of the silicon mounting platform and supports. The platform can thus be shaped to apply stresses to the resonator such that the minimum acceleration sensitivity is achieved. Second, a platform supported by flexible arms acts as a vibration isolation system, thus reducing the effective acceleration applied to the resonator. A study of a silicon micromachined isolation platform has been performed. Numerical analysis has been used to determine the effect of stress on the resonator, while a mass spring model has been used to predict the effective acceleration applied to the resonator.

The design of the silicon platform and supports determines the stresses applied to the resonator. Therefore, the platform design can be adjusted to induce stresses such that the minimum acceleration sensitivity is obtained. In order to determine the optimal platform design, a numerical analysis of the acceleration sensitivity of a STW resonator mounted on a silicon isolation system is performed. The isolation system also provides vibration isolation to the mounted resonator. The resonator and isolation platform are thus modeled as a mass-spring system with one degree of freedom to determine the effective vibration isolation. Combining the results of each analysis yields basic design guidelines for the fabrication of a micromachined vibration isolator.

Introduction

The reliable fabrication of small oscillators with low acceleration sensitivity ($10^{-10}/g$) is desired for a variety of military applications. Typically, to provide very low acceleration sensitivity requires the use of a vibration isolation system. This system increases the size of the oscillator, thus limiting the applications. The fabrication of a micromachined isolation system provides a solution to this problem.

Silicon micromachining allows precise fabrication of milli- and micro- sized mechanical systems with components having dimensions on the order of 1 micrometer. A study of the application of a micromachined silicon isolation platform to reducing acceleration sensitivity of a surface transverse wave (STW) resonator is presented here. The basic design of the resonator and the micromachined isolation system is shown in Fig 1.

Numerical Analysis

The calculation of the acceleration sensitivity of an isolated STW resonators is similar to the analysis of SAW resonators [1]. First the STW mode shape is calculated. Next, the isolation system with the attached resonator is parameterized and a finite element mesh is generated. An acceleration is applied to the mesh and the nodal displacements are calculated. The

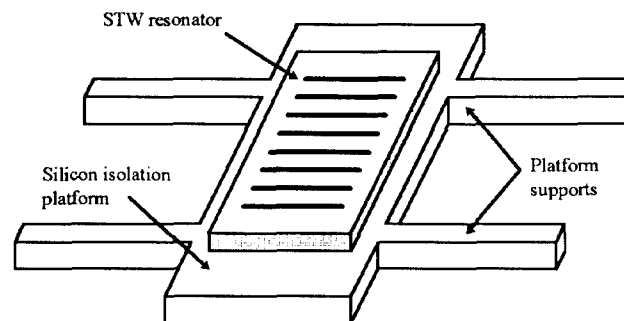


Figure 1. Illustration of a STW resonator mounted on a silicon isolation platform.

displacements provide the solution to the static biasing problem. Tiersten's perturbation integral [2] is used in conjunction with the STW mode shape and the spatially varying effective elastic constants determined from the static bias to numerically calculate the acceleration sensitivity of the STW resonator.

Solution of the Biasing State

The development of the static finite element equations for the solution of the biasing state begins with the general three dimensional equations of elasticity

$$T_{ij,i} + \rho b_i = 0 \quad (1)$$

$$S_{ij} = \frac{1}{2}(u_{i,j} + u_{j,i}) \quad (2)$$

$$T_{ij} = c_{ijkl} S_{kl} \quad (3)$$

where T_{ij} are the components of the stress tensor, b_i are the components of body force per unit volume, S_{ij} are the components of the infinitesimal strain tensor with u_i representing the components of displacement, c_{ijkl} are the components of the 2nd order elastic constant tensor, and ρ is the mass density of the material. The variational form, or weak form, of eqs. (1)-(3) is formulated for a body occupying a volume V bounded by a surface S as

$$\delta\Pi = \int_V T_{ij} \delta u_{j,i} dV - \int_V b_i \delta u_i dV - \int_S t_i \delta u_i dS = 0. \quad (4)$$

The finite element discretization process is applied by interpolating the displacements with a set of shape functions, N^q as follows:

$$u_j = N^q \bar{u}_j^q \quad (5)$$

where \bar{u}_j^q are the nodal displacements. In eq. (5) the superscripts are intended to imply a sum over nodes within an element or an entire mesh, depending upon the context. The shape functions N^q may take on several forms and will not be explicitly defined here. The reader is referred to references [3] and [4] for these and other finite element definitions. Using eq. (5) in the functional (4) gives

$$\delta\Pi = \left[\int_{\Omega} \frac{\partial N^p}{\partial x_i} c_{ijkl} \frac{\partial N^q}{\partial x_l} d\Omega \bar{u}_k^q - \int_{\Omega} b_j N^p d\Omega - \int_{\Gamma} t_j N^p d\Gamma \right] \delta \bar{u}_j^p = 0. \quad (6)$$

Here Ω represents the discretized domain and Γ the bounding surface. For arbitrary variations, $\delta \bar{u}_j^p$, eq. (6) reduces to

$$K_{jk}^{pq} \bar{u}_k^q - F_j^p = 0 \quad (7)$$

with the elemental equation

$$k_{jk}^{pq} = c_{ijkl} G_{il}^{pq} \quad (8)$$

where K_{jk}^{pq} and F_j^p are the global stiffness matrix and load vector, with k_{jk}^{pq} and f_j^p the corresponding element or local quantities, and

$$G_{il}^{pq} = \int_{\Omega} \frac{\partial N^p}{\partial x_i} \frac{\partial N^q}{\partial x_l} d\Omega_l \quad (9)$$

and

$$f_j^p = \int_{\Omega_l} b_j N^p d\Omega_l + \int_{\Gamma_l} t_j N^p d\Gamma_l \quad (10)$$

Here Ω_l represents the single element domain with bounding surface Γ_l . The global system gives rise to the matrix problem

$$\tilde{K} \tilde{u} = \tilde{F} \quad (11)$$

with solution

$$\tilde{u} = \tilde{K}^{-1} \tilde{F} \quad (12)$$

Solution of STW Mode Shape

Shown in Fig. 2 is the general coordinate system and dimensions used for the development of the surface transverse wave solution. The STW mode shape is calculated by expanding the u_1 displacement in an infinite Floquet series of space harmonics as [5-7]

$$u_1 = \sum_{n=-\infty}^{+\infty} A_n e^{i\alpha_n x_2} e^{i\beta_n x_3} e^{i\alpha x_1} \quad (13)$$

where

$$\beta_n = \beta + \frac{2\pi n}{\Lambda} \quad (14)$$

is the n^{th} space harmonic propagation constant, with β the Floquet wave propagation constant, α_n is the

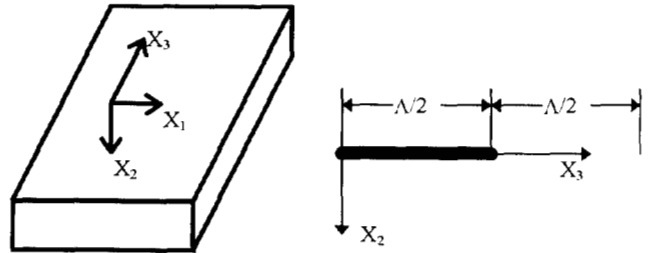


Figure 2. Coordinate system and dimensions for surface transverse wave calculations.

(complex) propagation constant into the substrate, Λ is the grating period, ω is the angular frequency, and A_n is the amplitude of the n^{th} space harmonic. Using eq. (13) in the wave equation resulting from eqs. (1)-(3)

$$c_{ijkl} u_{k,li} - \rho \ddot{u}_j = 0 \quad (15)$$

yields the following polynomial equation

$$\alpha_n^2 c_{66} + 2\alpha_n \beta_n c_{56} + \beta_n^2 c_{55} - \rho \omega^2 = 0 \quad (16)$$

For given values of β and ω , eq. (16) can be solved for two roots

$$\alpha_n = -\frac{c_{56}}{c_{66}} \beta_n \pm \sqrt{\frac{\rho \omega^2}{c_{66}} - \frac{\bar{c}}{c_{66}} \beta_n^2} \quad (17)$$

where

$$\bar{c} = (c_{55} c_{66} - c_{56}^2) / c_{66} \quad (18)$$

Since the resulting solution must decay in x_2 , only one root of eq. (16) is retained, namely the one with a positive imaginary part. This root may be written as

$$\alpha_n = -\frac{c_{56}}{c_{66}} \beta_n + i \sqrt{\frac{\bar{c}}{c_{66}} \beta_n^2 - \frac{\rho \omega^2}{c_{66}}} \quad (19)$$

where it is understood that the quantity under the square root is always taken in absolute value.

For an electrode of length $\Lambda/2$, with electrode material density ρ and thickness h , the relevant traction boundary condition at $x_2 = 0$, is given by the Datta-Hunsinger relation [8]

$$T_{12} = \begin{cases} \rho h \ddot{u}_1 - h \frac{\partial T_{13}}{\partial x_3} & \text{on } 0 \leq x_3 < \frac{\Lambda}{2} \\ 0 & \text{on } \frac{\Lambda}{2} \leq x_3 < \Lambda \end{cases} \quad (20)$$

In eq. (20) the term T_{13} represents the 1-3 component of stress in the electrode

$$T_{13} = \mu' u_{1,3} \left[H\left(x_3 - \frac{\Lambda}{2}\right) - H(x_3) \right] \quad (21)$$

where μ' is the shear modulus of the electrode material (assumed here to be isotropic) and $H(x_3)$ represents the Heaviside step function. Substituting eq. (13) into eq. (20) and making use of orthogonality gives

$$i \{ \alpha_q c_{66} + \beta_q c_{56} \} A_q = \frac{1}{\Lambda} \sum_{n=-\infty}^{+\infty} \int_0^{\Lambda/2} \{ -\rho' \omega^2 h + h \mu' \beta_n^2 - i \mu' \beta_n \left[\delta\left(x_3 - \frac{\Lambda}{2}\right) - \delta(x_3) \right] \} A_n e^{i(\beta_n - \beta_q)x_3} dx_3 \quad (22)$$

where $\delta(x_3)$ is the Dirac delta function. Eq. (22) is simplified by introducing the following dimensionless quantities

$$\bar{\beta} = \frac{\Lambda}{\pi} \beta, \quad \bar{\beta}_n = \frac{\Lambda}{\pi} \beta_n, \quad \bar{\omega} = \frac{\Lambda}{\pi} \omega \sqrt{\bar{c}/\rho}, \quad R = \frac{\rho'}{\rho}, \quad \kappa = \frac{\mu'}{\bar{c}}, \quad p = \frac{h}{\Lambda}, \quad \text{and } k = \sqrt{c_{66}/\bar{c}} \quad (23)$$

to give

$$\sum_{n=-\infty}^{n=\infty} D_{qn} A_n = 0 \quad \text{for } q = 0, \pm 1, \pm 2, \dots, \quad (24)$$

where

$$D_{qn} = \begin{cases} ip \left[\frac{1 - (-1)^{(n-q)}}{2(n-q)} \right] [R \bar{\omega}^2 - \kappa \bar{\beta}_n \bar{\beta}_q] & \text{for } n \neq q \\ \frac{\pi}{2} p [R \bar{\omega}^2 - \kappa \bar{\beta}_n^2] - k \sqrt{\bar{\beta}_n^2 - \bar{\omega}^2} & \text{for } n = q \end{cases} \quad (25)$$

For a finite truncation of the series, say to N terms, eq. (24) is rendered as a set of $2N+1$ equations in $2N+1$ unknowns, which can be expressed by the matrix equation

$$\tilde{D} \tilde{A} = 0 \quad (26)$$

For a non-trivial solution to Eq. (26), the determinant of the coefficient matrix must vanish

$$|\tilde{D}| = 0 \quad (27)$$

which yields the frequency equation for STW propagation. The general procedure for determining a solution for a given $\bar{\beta}$ is to select a trial $\bar{\omega}$, compute the matrix components via eq. (25), and compute its determinant. The value of $\bar{\omega}$ is updated accordingly (i.e., using bisection) until a sufficiently converged root to eq. (27) is obtained. Once a root is found, the amplitude ratios of the space harmonics can be determined by solving for the null space of the now singular eq. (26).

Calculation of the Frequency Shift

The frequency shift under a given static biasing state is computed using Tiersten's perturbation method [2] for small fields superposed on a bias [9]. The change in resonant frequency of the μ^{th} eigen-mode is given as

$$\Delta_\mu = H_\mu / 2\omega_\mu \quad (28)$$

where

$$H_\mu = - \int_V \hat{c}_{L\gamma M\alpha} g_{\alpha,M}^\mu g_{\gamma,L}^\mu dV \quad (29)$$

is the integral over the volume, V , of the normalized mode shape g , and the spatially varying effective elastic constants

$$\begin{aligned} \hat{c}_{L\gamma M\alpha} = & T_{LM}^1 \delta_{\gamma\alpha} + c_{L\gamma\alpha MAB} E_{AB}^1 \\ & + c_{L\gamma NM} w_{\alpha,N} + c_{LN\alpha M} w_{\gamma,N}. \end{aligned} \quad (30)$$

The spatially varying constants, $\hat{c}_{L\gamma M\alpha}$, are derived from the biasing state with T_{LM}^1 the biasing stresses, E_{AB}^1 the biasing strains, and $w_{\gamma,N}$ the biasing deformation gradients. The constants $c_{L\gamma\alpha MAB}$ denote the 3rd order elastic constants for the material.

The perturbation integral (29) is evaluated as a sum over N elements as

$$H_\mu = - \sum_{i=1}^N \int_{\Omega_i} \hat{c}_{L\gamma M\alpha} g_{\alpha,M}^\mu g_{\gamma,L}^\mu d\Omega_i \quad (31)$$

where Ω_i denotes the volumetric domain of the i^{th} element. To evaluate eq. (31) the necessary quantities need to be sampled at a specific point, (η_1, η_2, η_3) , in the interior of the element domain. This can be achieved by using the solution vector with eq. (5) to obtain

$$E_{ij}^1(\eta_1, \eta_2, \eta_3) = \frac{1}{2} \left(\frac{\partial N^p}{\partial x_j} \bar{u}_i^p + \frac{\partial N^p}{\partial x_i} \bar{u}_j^p \right) \quad (32)$$

and

$$\Omega_{ij}^1(\eta_1, \eta_2, \eta_3) = \frac{1}{2} \left(\frac{\partial N^p}{\partial x_j} \bar{u}_i^p - \frac{\partial N^p}{\partial x_i} \bar{u}_j^p \right) \quad (33)$$

where Ω_{ij}^1 are the biasing rotations. It should be noted that E_{ij}^1 and Ω_{ij}^1 are sampled in the interior of the element domain where they are accurate. In general these quantities should not be considered accurate at nodal points or along element edges. Using eqs. (32) and (33), the deformation gradients at the element domain point (η_1, η_2, η_3) are given as

$$w_{i,j}(\eta_1, \eta_2, \eta_3) = E_{ij}^1(\eta_1, \eta_2, \eta_3) + \Omega_{ij}^1(\eta_1, \eta_2, \eta_3) \quad (34)$$

The biasing stresses, T_{LM}^1 , at this point are then computed using eq. (3) and all are combined via eq. (30) to produce values of the components of $\hat{c}_{L\gamma M\alpha}$ at a point in the interior of the element under consideration.

A single element integral of eq. (31) is computed by first subdividing the element into $m_1 \times m_2 \times m_3$ smaller sub-elements and sampling the $\hat{c}_{L\gamma M\alpha}$ terms at the centroid of each sub-domain. For a small enough domain, it may be assumed that the $\hat{c}_{L\gamma M\alpha}$ terms are approximately constant, which leads to the approximation

$$\begin{aligned} \int_{\Omega} \hat{c}_{L\gamma M\alpha} g_{\alpha,M}^\mu g_{\gamma,L}^\mu d\Omega \approx \\ \sum_i^{m_1} \sum_j^{m_2} \sum_k^{m_3} \hat{c}_{L\gamma M\alpha}(\eta_1^{(i)}, \eta_2^{(j)}, \eta_3^{(k)}) \int_{\Omega^{(i,j,k)}} g_{\alpha,M}^\mu g_{\gamma,L}^\mu d\Omega^{(i,j,k)} \end{aligned} \quad (35)$$

where $(\eta_1^{(i)}, \eta_2^{(j)}, \eta_3^{(k)})$ denotes the centroid of the (i^{th}, j^{th}, k^{th}) sub-element domain $\Omega^{(i,j,k)}$ under consideration. The integral $\int_{\Omega^{(i,j,k)}} g_{\alpha,M}^\mu g_{\gamma,L}^\mu d\Omega^{(i,j,k)}$ in eq. (35) is evaluated

exactly using the form given by Eq. (13).

Numerical Results

An analysis is done using a 1GHz STW resonator on ST-cut quartz. The resonator is 1.87 mm wide, 3.97 mm long, and 0.51 mm thick. The silicon platform and supports are of uniform thickness, t . The platform model parameters, inset, i ; overhang, oh ; support length, s_i ; and support width, s_w are defined as shown in Fig. 3. The resonator is assumed to be rigidly mounted onto the silicon support platform.

After calculating the STW mode shape, a $1/4$ model finite element mesh is generated to perform the analysis. This mesh is shown in Fig. 4. Due to the symmetry of the problem, it is only necessary to perform the finite element analysis on $1/4$ of the model, thus significantly reducing the computational resources required. For all computations, a 1g normal acceleration is applied to the mesh and the nodal displacements are calculated. The $1/4$ model is then mirrored around the symmetric axes to form a complete model as seen in Fig. 5. Finally the acceleration sensitivity is computed using Tiersten's perturbation integral. To ensure sufficient accuracy, convergence studies were performed over the number of terms in the STW mode shape, the number and allocation of nodes in the mesh, and the number of

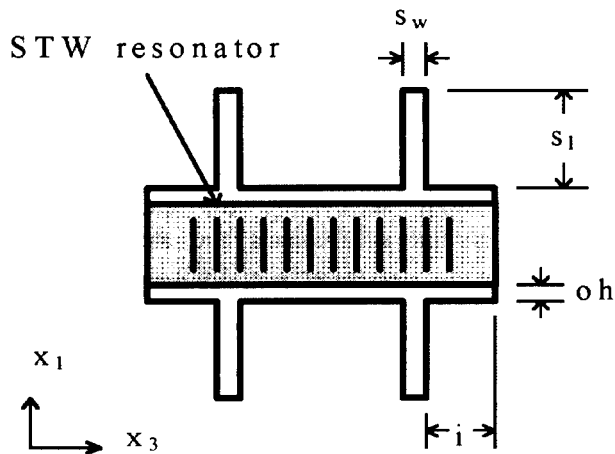


Figure 3. Model parameters for the silicon isolation system.

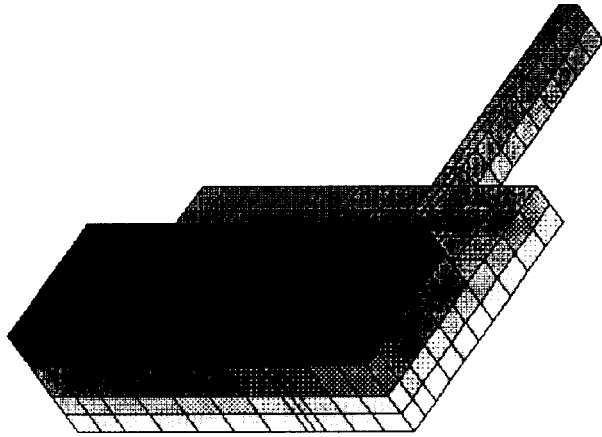


Figure 4. A finite element mesh of $\frac{1}{4}$ of the model.

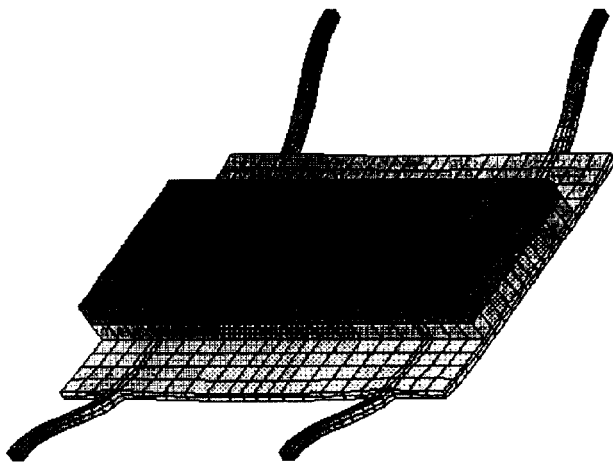


Figure 5. Three dimensional plot of the mesh after performing the finite element analysis and mirroring the model about the symmetric axes.

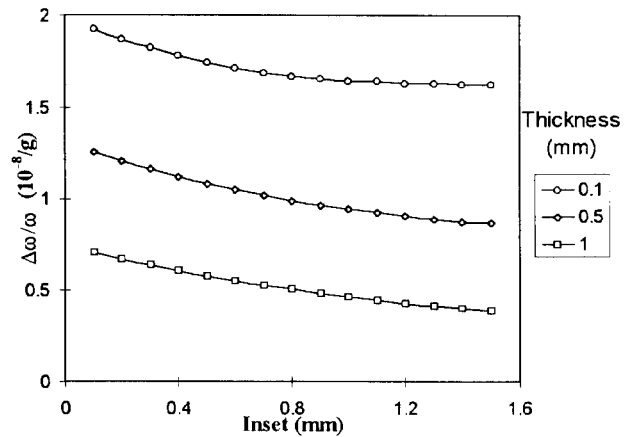


Figure 6. The effect of support location on acceleration sensitivity. Data is presented for 3 different silicon thickness values.

approximation cells in the active area. The platform model parameters i , t , oh , s_l , and s_w were varied over a range of values and the acceleration sensitivity of the resonator calculated. Unless otherwise specified, the parameters are defined as $i = 1.0$ mm, $t = 0.4$ mm, $oh = 0.573$ mm, $s_l = 2.00$ mm, and $s_w = 0.05$ mm.

The effect of the inset on acceleration sensitivity is shown in Fig. 6. Increasing the inset moves the supports closer to the center of the resonator. Fig. 7 shows the deformation of the resonator along the x_3 direction for several inset values. It is clear that the deformation at the center of the resonator decreases as the supports are moved towards the center while the deformations at the ends of the resonator initially decrease, but then increase rapidly. It is also apparent that at some point the deformation at the center of the resonator begins to increase again. The point at which

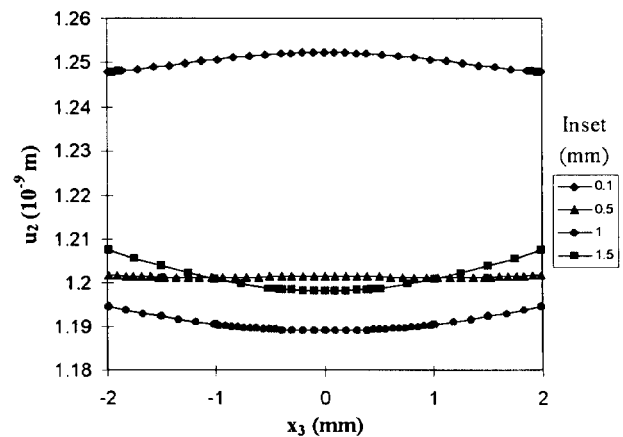


Figure 7. Deformation along x_3 at $x_1 = x_2 = 0$ for several inset values.

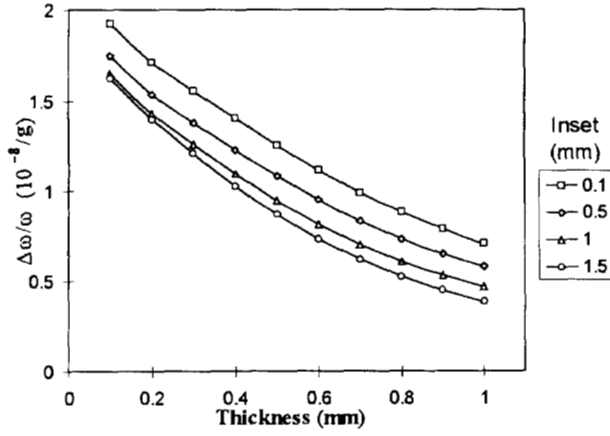


Figure 8. The effect of platform and support thickness on acceleration sensitivity.

this crossover occurs results in a minimum acceleration sensitivity value. However, the inset value at which this occurs increases as the platform gets thicker. It has been shown that changes in the acceleration sensitivity are caused by deformation of the crystal [11], and therefore it is not surprising that the acceleration sensitivity of the resonator also decreases as the inset is increased.

Figure 8 shows the effect of thickness on acceleration sensitivity. Increasing the thickness provides a more rigid support for the resonator and thus decreases the deformation. Again, this directly leads to decreased acceleration sensitivity.

The effect of platform overhang is shown in Fig. 9. As is seen, increasing the overhang leads to an increased acceleration sensitivity. The effects of support width and support length are shown in Figs. 10 and 11, respectively. The support width has minimal effect on

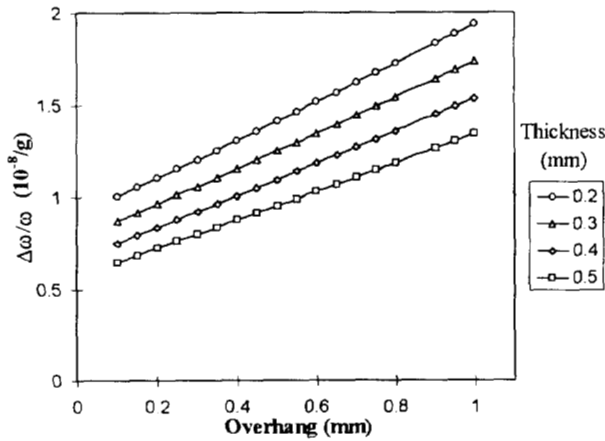


Figure 9. The effect of platform overhang on acceleration sensitivity. Note, inset = 0.8 mm.

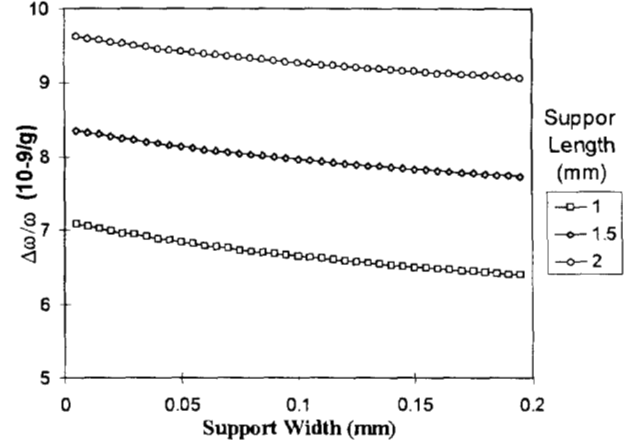


Figure 10. The effect of support width on acceleration sensitivity.

acceleration sensitivity, while increasing support length leads to increased acceleration sensitivity

Vibration Isolation

Determining the effective acceleration applied to the resonator is done by modeling the isolation platform and resonator as a mass-spring system with a single degree of freedom. This is illustrated in Fig. 12, where k_{sys} is the effective spring constant of the supports, S is the damping coefficient, and M_0 is the mass of the resonator and the silicon support platform. The mass is simply computed as

$$M_0 = M_{STW} + M_{Platform} \quad (36)$$

where M_{STW} is the mass of the STW resonator and $M_{Platform}$ is the mass of the silicon platform. The effective

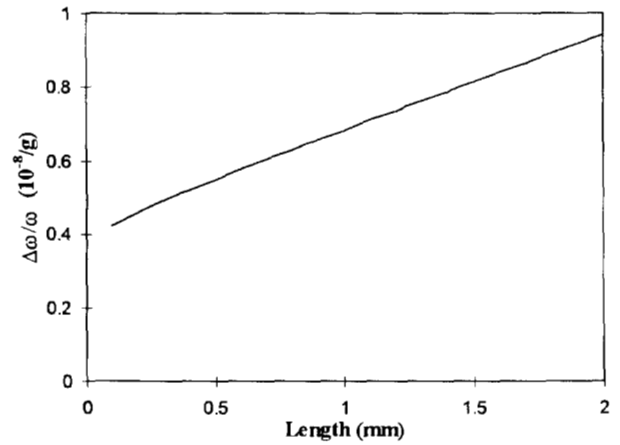


Figure 11. The effect of support length on acceleration sensitivity.

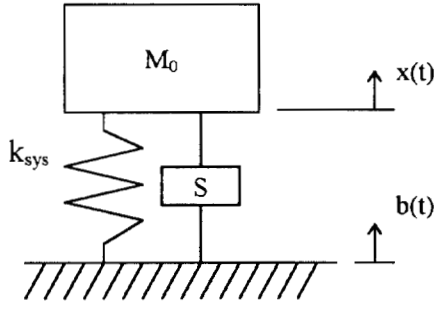


Figure 12. Single degree of freedom mass-spring system with viscous damping.

mass of the support arms is much less than M_0 and is therefore neglected. The spring constant for all four supports, k_{sys} , is equal to the sum of the spring constants of each of the four beams. Since the dimensions of the beams are identical, $k_{sys} = 4 \times k_{beam}$, where k_{beam} is the spring constant of one support. The spring constant of the beam is computed as [12]

$$k_{beam} = k_1 + k_2 + k_3 \quad (37)$$

where k_1 is the spring constant do to bending of the beam, k_2 , is the spring constant do to residual stress in the material, and k_3 is the spring constant do to bending stress in the deformed beam. The low doped (110)-cut single crystal-silicon used in fabricating the beams has very low residual stress, and thus k_2 can be neglected. Further, for small deflections, k_3 is also negligible. Therefore, the effective spring constant becomes [12]

$$k_{beam} = k_1 = E_{Si} \frac{s_w t^3}{s_l^3} \quad (38)$$

where E_{Si} is the Young's modulus of silicon, s_w is the width of the supports, t is the thickness of the supports, and s_l is the length of the support.

Calculation of System Response

In this analysis, we are concerned with the absolute transmissibility of the acceleration from the base to the mass, or

$$T_A = \frac{x}{b} = \frac{\dot{x}}{\dot{b}} = \frac{\ddot{x}}{\ddot{b}} \quad (39)$$

where T_A is the absolute transmissibility, x , \dot{x} , \ddot{x} , b , \dot{b} , and \ddot{b} are the displacement, velocity and acceleration of the mass and base, respectively. Note that from Fig. 12 up is defined as the positive direction for both x and b . A

simple harmonic vibration applied to the base is written as

$$b(t) = B_0 \sin(\omega t). \quad (40)$$

The force applied to the mass is then

$$f_{applied} = -(f_s + f_D) \quad (41)$$

where f_s is the force from the spring and f_D is the damping force. The spring force is computed from the well known spring equation

$$f_s = k_{sys} \delta = k_{sys} (x(t) - B_0 \sin(\omega t)) \quad (42)$$

while the damping force is proportional to the velocity of the displacement, or

$$f_D = S \dot{\delta} = S (\dot{x}(t) - B_0 \omega \cos(\omega t)) \quad (43)$$

Substituting eqs. (42) and (43) into eq. (41) and combining with the classical acceleration equation $f = ma$ yields

$$M_0 \ddot{x}(t) + k_{sys} (x(t) - B_0 \sin(\omega t)) + S (\dot{x}(t) - B_0 \omega \cos(\omega t)) = 0 \quad (44)$$

Equation (44) can be rearranged as

$$M_0 \ddot{x}(t) + S \dot{x}(t) + k_{sys} x(t) = \sqrt{(k_{sys} B_0)^2 + (S B_0 \omega)^2} \sin(\omega t + \varepsilon) \quad (45)$$

Let $x(t) = A \sin(\omega t)$, then $\dot{x}(t) = A \omega \cos(\omega t)$, and $\ddot{x}(t) = -A \omega^2 \sin(\omega t)$. Substituting these into Eq. (45) and rearranging yields

$$A \sqrt{(k_{sys} - M_0 \omega^2)^2 + (S \omega)^2} = B_0 \sqrt{k_{sys}^2 + (S \omega)^2} \quad (46)$$

Dividing through and rearranging results in

$$T_A = \frac{A}{B_0} = \sqrt{\frac{1 + \left(\frac{S}{M_0} \frac{\omega}{\omega_c}\right)^2}{\left(1 - \frac{\omega^2}{\omega_c^2}\right)^2 + \left(\frac{S}{M_0} \frac{\omega}{\omega_c}\right)^2}} \quad (47)$$

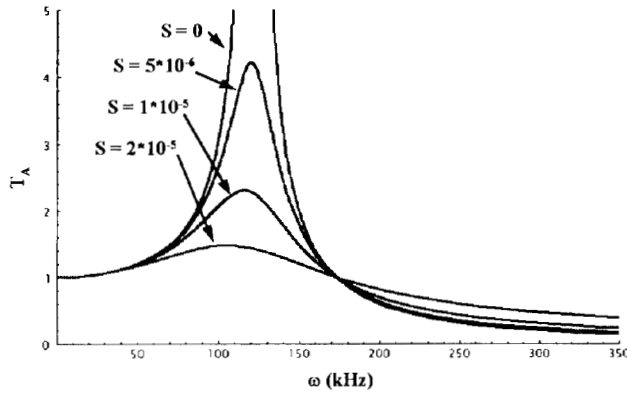


Figure 13. Absolute transmissibility of a base acceleration to a supported resonator.

where

$$\omega_c = \sqrt{k_{sys} / M_0} \quad (48)$$

is the resonant frequency of the system.

Using eqs. (36), (38), and (47), the response of the silicon isolation platform and the STW resonator to a vibration of the platform base can now be calculated. For a silicon isolation platform with $s_w = 0.05$ mm, $s_l = 2$ mm, $t = 0.40$ mm, and $M_0 = 2.03 \times 10^{-5}$ kg, the spring constant is calculated as $k_{sys} = 304 \times 10^3$ kg/s², and the resonant frequency is calculated as $\omega_c = 122.4$ kHz. Figure 13 shows the transmissibility for this platform.

It is clear from Fig. 13 that as ω increases above the resonant frequency the acceleration passed from the base to the resonator decreases. It is desirable that the resonant frequency of the system be significantly lower than the range of the vibration that the system is subjected to. As can be seen, the resonant frequency of this system is very high. Equation (48) shows that ω_c is directly proportional to the square root of the spring constant, k_{sys} , and inversely proportional to the square root of the mass M_0 . Combining this with eq. (38) generates the relationships between the system design parameters and the resonant frequency as

$$\omega_c \propto t_{sup}^{(3/2)} s_l^{-(3/2)} \quad (48)$$

$$\omega_c \propto s_w^{(1/2)} M_0^{-(1/2)}$$

where t_{sup} is the support thickness. It is clear that a significant reduction in ω_c requires that the support length be increased while support thickness is decreased. To a lesser degree, the mass and support width can also be used to decrease the resonant frequency. By decoupling the support thickness from the platform

thickness we can significantly decrease ω_c without decreasing the rigidity of the platform support.

Conclusions

An analysis of a micromachined silicon isolation system has been performed. Combining the results from numerical analysis of the system under a static load with the vibration isolation analysis yields several conclusions. First, the support beams should be located near the center of the structure to properly distribute stress across the platform. Second, the support platform should be made as thick as possible to provide a rigid support to the resonator. Third, to provide effective vibration isolation, the supports must be made longer and thinner. Therefore, it is necessary to decouple the support thickness from the platform thickness. This will allow the platform thickness to be increased providing the desired rigid support, while still allowing the support thickness to be decreased to reduce the systems resonant frequency.

Acknowledgments

This work was supported in part by a grant of high performance computing time from the Department of Defense High Performance Computing Center. Computational runs were performed on the Vicksburg Center Cray C90 (pk@wes.army.mil).

References

- [1] J.T. Stewart, J.A. Kosinski, and A. Ballato, "An Analysis of the Dynamic Behavior and Acceleration Sensitivity of a SAW Resonator Supported by Flexible Beams," *Proc. 1995 IEEE International Frequency Control Symposium*, pp. 507-513.
- [2] H.F. Tiersten, "Perturbation Theory for Linear Electroelastic Equations for Small Fields Superposed on a Bias," *J. Acoust. Soc. Am.*, Vol. 64, pp. 832-837, 1978.
- [3] T.J.R. Hughes, *The Finite Element Method, Linear Static and Dynamic Analysis*, Prentice Hall, 1987.
- [4] O.C. Zienkiewicz and R.L. Taylor, *The Finite Element Method*, Vols. 1 & 2, McGraw-Hill, 1989.
- [5] D.F. Thompson and B.A. Auld, "Surface Transverse Wave Propagation Under Metal Strip Gratings," *Proc. 1986 Ultrasonics Symposium*, pp. 261-266.

[6] C.A. Flory and R.L. Baer, "Surface Transverse Wave Mode Analysis and Coupling to Interdigital Transducers," Proc. 1987 Ultrasonics Symposium, pp. 313-318.

[7] S. Ballandras, E. Gravignat, and E. Bigler, "Single and Double Side Grating Devices Built on Thin Quartz Plates for the Excitation of Surface Transverse Waves," Proc. 1995 Ultrasonics Symposium, pp. 335-340.

[8] S. Datta and B.J. Hunsinger, "First-order Reflection Coefficient of Surface Acoustic Waves from Thin-strip Overlays," J. Appl. Phys., Vol. 50, pp. 5661-5665, Sept. 1979.

[9] J.C. Baumhauer and H.F. Tiersten, "Nonlinear Electroelastic Equations for Small Fields Superposed on a Bias," J. Acoust. Soc. Am., Vol. 54, pp. 1017-1034, 1973.

[10] B.K. Sinha and H.F. Tiersten, "An Analysis of Transverse Modes in Acoustic Wave Resonators," J. Appl. Phys., Vol. 51, pp. 3099-3112, June 1980.

[11] J.A. Kosinski, A. Ballato, "Designing for Low Acceleration Sensitivity," IEEE Transactions on Ultrasonics, Ferroelectrics, and Frequency Control, Vol. 40, pp.532-537, Sept. 1993.

[12] R. Howe, A. Pisano, and B. Boser, Monolithic Surface Micromachined Inertial Sensors Course Notes. San Francisco, UC Berkeley, 1995.

[13] W. K. Wilson, Vibration Engineering, Charles Griffin & Company Limited, London, 1959.

[14] J. E. Ruzika and T. F. Derby, Influence of Damping in Vibration Isolation, The shock and vibration information center, United States Department of Defense, 1971.